

Onsager mechanism of photogeneration in amorphous selenium

D. M. Pai and R. C. Enck

Xerographic Technology Department, Joseph C. Wilson Center for Technology, Xerox Corporation, Webster, New York 14580
(Received 27 January 1975)

The Onsager theory of dissociation has been used to explain the electric field, excitation wavelength, and temperature dependence of photogeneration in amorphous selenium. The Onsager theory was formulated to explain the departure from Ohmic behavior in either weak electrolytes or solid dielectrics, and the analysis of charge separation was carried out using the theory of Brownian motion of one particle under the action of Coulomb attraction and the collecting field. Both the absolute magnitude and functional dependence on electric field of the photogeneration efficiency in amorphous selenium at any excitation wavelength can be unambiguously explained using a single parameter which is the initial separation between thermalized electron-hole pairs. This initial separation varies from 7.0 nm at 400-nm excitation to 0.84 nm at 620-nm excitation. The application of the theory to the measured photogeneration data also leads to the important conclusion that each absorbed photon creates a pair of thermalized carriers bound by their mutual Coulomb attraction. The low quantum efficiency measured for long-wavelength excitation is due to the smaller initial separation between oppositely charged thermalized pairs of carriers resulting in smaller dissociation efficiency. Good agreement is also obtained between the measured temperature dependence of the photogeneration efficiency and that predicted by the theory.

I. INTRODUCTION

The experimental data on optical absorption and photogeneration in amorphous selenium have been the subject of several varied interpretations.¹⁻⁵ The efficiency of photoinjection of carriers from the absorption region into the bulk of the material is close to unity at 400 nm and decreases continuously as the wavelength is increased although the absorption is complete at these wavelengths. The efficiency of photoinjection takes into account both the photogeneration process and any loss in the photogeneration region. The variation of efficiency with wavelength was first explained² on the basis of dual absorption in that at each wavelength there were distinctly two types of absorption, each with a different set of initial and final states. One of these absorptions was assigned a unity quantum efficiency (QE) of generation and the other a zero QE; hence, a low QE at any wavelength could be explained on the basis of a higher proportion of absorption with zero QE.

Later measurements revealed³ that the efficiency of photoinjection varied with the applied electric field and was thermally activated with an activation energy that decreased as the exciting photon energy was increased. It was thought that the photoelectric properties of amorphous selenium were those of a molecular solid, with the photoabsorption producing a local excitation in the form of a bound electron-hole pair which dissociated or recombined under the combined influence of thermal excitation and applied electric field.³ The expression that was used to explain this field dependence was the one derived by Frenkel,⁶ sometimes known as the

Poole-Frenkel (PF) expression.

The PF expression, even with the introduction of a parameter describing geminate recombination,⁴ has been found to be inadequate in providing a satisfactory explanation of the photogeneration data and the measured activation energies. At long wavelengths where the agreement between the experimental results and the PF expression is by far the best, the slope of the efficiency variation with electric field is a factor of 2 different from that predicted theoretically.³ No attempt has been made to examine the serious disagreement between the theory which explains the experimental data on the basis of dual absorption and the explanation based on the PF effect.

We believe Onsager's theory⁷ provides a completely satisfactory explanation of the experimental results on photogeneration in this material. Onsager computed the effect of an external field on electrolytic dissociation from the equations of Brownian motion in the presence of Coulombic attraction. As can be expected, the efficiency of dissociation depends on the initial distance between the oppositely charged carriers. The absolute value and the functional dependence of the photogeneration efficiency with the electric field can be completely explained using the initial distances between the carriers as a parameter. The temperature dependences of the photogeneration efficiencies calculated using these same distances are in good agreement with the measured activation energies. This theory also leads to the conclusion that every absorbed photon creates a pair of thermalized carriers bound by their mutual Coulombic attraction. The low quantum efficiency

at long wavelength is due to a shorter starting distance between the carriers, resulting in a smaller dissociation efficiency.

II. EXPERIMENTAL PROCEDURE

The measurement of photoinjection efficiency is carried out by two different techniques, each with its own distinct advantages. The first is the xerographic discharge technique which measures the rate of discharge of a corona-charged amorphous selenium film under steady illumination. The second is the measurement of the transient photoconductivity using flash illumination on a sandwich cell arrangement. The former has the advantage that the measurement can be performed up to about 6×10^7 V/m, whereas in the latter measurement breakdown generally occurs at about 2×10^7 V/m. However, the latter allows the transport to be easily time resolved and is more suitable when the temperature is to be varied.

The amorphous selenium films were prepared by vacuum evaporation of high-purity selenium from an open boat at 250°C onto aluminum substrates maintained at 55°C . The vacuum is generally in the neighborhood of 5×10^{-5} Torr. Films varying in thickness from 3 to 50 μm were used in the measurements. For transient photoconductivity measurements, the sandwich cell configuration is obtained by evaporating a semitransparent gold electrode on top of the selenium film.

The xerographic discharge technique consists of corona-charging the film to the required voltage and then discharging it under steady-state monochromatic illumination [Fig. 1(a)]. The voltage on the film is measured by a probe which is capacitively coupled to the plate. The output from the probe is fed through an amplifier to a recorder. The measured quantity is the initial discharge rate which is dV/dt at $t=0$.

For all the exciting wavelengths used in our investigation the absorption coefficient is high ($> 10^6 \text{ m}^{-1}$), so that all the light is absorbed in a thin surface region ($< 1 \mu\text{m}$) of films which are at least microns thick. To measure the photoinjection efficiency of holes, the film is corona charged positively. In the absence of loss of carriers through deep bulk trapping, each carrier that is emitted into the bulk drifts to the substrate, and the rate of discharge of the film is given by

$$C \frac{dV}{dt} = \eta I e, \quad (1)$$

where C is the geometrical capacitance of the film, dV/dt is the rate of change of voltage with time, η is the number of free carriers emitted into the bulk per absorbed photon (equal to the number of photogenerated free carriers per absorbed photon in the absence of any loss due either to surface re-

combination or recombination in the absorption region), I is the light intensity in photons/sec, and e is the electronic charge.

Equation (1) can be rewritten for unit area as

$$\frac{dE}{dt} = \frac{\eta I e}{\kappa \epsilon_0} \quad \text{OR} \quad \eta = \frac{\kappa \epsilon_0 (dE/dt)}{I e}, \quad (2)$$

where κ is the relative dielectric constant of amorphous selenium and ϵ_0 is the permittivity of free space. At sufficiently low applied voltages, when the transit time of the carriers becomes comparable to the deep bulk trapping lifetime, some of the carriers that are emitted into the bulk are trapped; hence their contribution to the discharge is correspondingly less. It can be easily shown that the rate of discharge in the presence of bulk trapping is given by

$$\frac{dE}{dt} = \frac{\eta I e}{\kappa \epsilon_0} \frac{\mu E \tau}{L} (1 - e^{-L/\mu E \tau}), \quad (3)$$

where τ is the bulk trapping lifetime.

For applied fields such that $\mu E \tau \ll L$,

$$\frac{dE}{dt} = \frac{\eta I e}{\kappa \epsilon_0} \frac{\mu E \tau}{L}. \quad (4)$$

The rate of discharge of the film for constant applied field is inversely proportional to the thickness of the film. Hence, the appearance of bulk

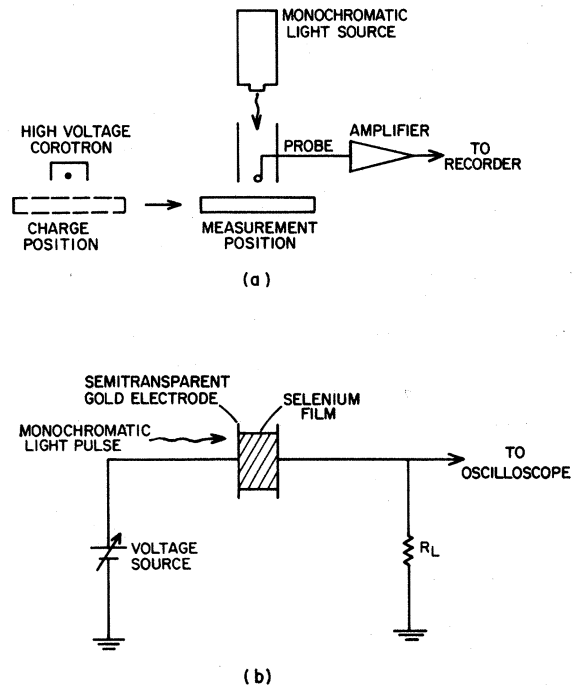


FIG. 1. (a) Schematic of the experimental arrangement for measuring quantum efficiency of photoinjection by xerographic discharge technique. (b) Schematic of the experimental setup using the electroded structure.

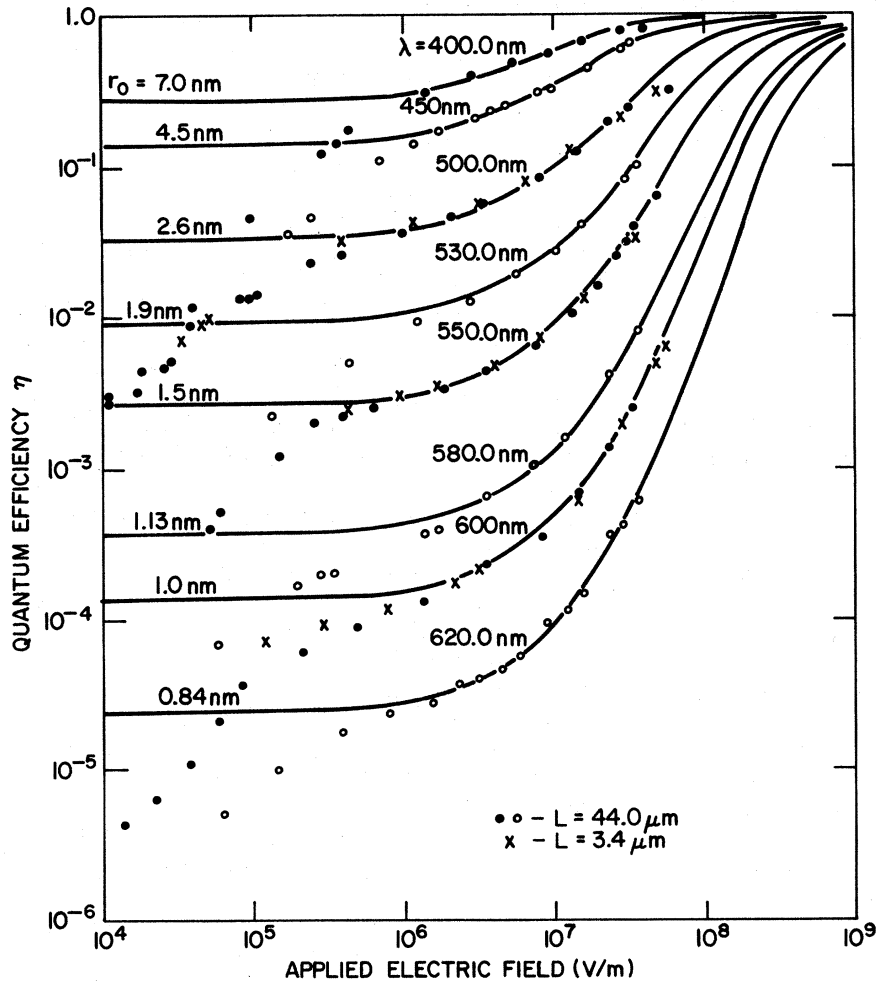


FIG. 2. Circles and crosses show the experimental quantum efficiency of photoinjection of holes vs applied electric field for different values of the wavelength of exciting radiation. Figure also shows data on films of two different thicknesses. Solid lines are the theoretical Onsager dissociation efficiencies for $\phi_0 = 1$ and for initial separation r_0 indicated in the figure.

trapping can be detected by measuring the rate of discharge of the applied voltage as a function of film thickness.

The setup used for transient photoconductivity experiment with a sandwich cell configuration is shown in Fig. 1(b) and has been described previously by a number of workers.^{2-4,8-10} The principle behind this technique is that the carriers generated by a light flash absorbed in a thin layer close to the top electrode drift to the appropriate electrode. A voltage proportional to the number of charges drifting appears across the resistance R .

III. EXPERIMENTAL RESULTS

In Fig. 2, the data points represent the QE measured with the xerographic technique on films of 3.4- and 44.0- μm thickness as a function of the applied electric field for light of eight different exciting wavelengths. Since the films are corona charged positively, the discharge is caused by holes drifting from the photogeneration region near the top of the film to the substrate. For some wavelengths, the discharge rates are plotted

for two different film thicknesses to determine whether there is any loss of holes due to bulk trapping. For fields larger than about 2×10^5 V/m, the two films within experimental error have identical sensitivities, indicating from Eqs. (1) and (2) that bulk trapping is not present in this region. The low-field region ($\leq 5 \times 10^5$ V/m) is most vulnerable from a standpoint of experimental inaccuracies. A small amount of trapped charge results in a field in the generation region that is vastly different from the applied field V/L . The film must be "rested" for several days between measurements to get this small charge out of the system. Under the usual conditions of a few minutes of resting between measurements, a large error can be expected at low applied fields. The discussion will therefore be confined to the field region larger than about 5×10^5 V/m.

There are several features that characterize the sensitivity curves of Fig. 2.

(i) Since there is no "permanent" bulk trapping, the shape of the curves directly displays the electric field dependence of the photoinjection efficiency.

(ii) The shape of the electric field dependence of QE for the short-wavelength region of the spectrum is vastly different from that in the long-wavelength region. In the blue region, QE varies approximately linearly with electric field for fields less than 10^6 V/m, changing to sublinear (between $E^{0.3}$ and $E^{0.5}$) for fields larger than 10^6 V/m. In the red region of the spectrum, the QE rises sharply for field larger than about 10^7 V/m and tends to saturate in the intermediate field region. A dropoff from saturation appears at lower fields, and the field at which it occurs is substantially lower than the field at which the drop is observed in the blue region. This dropoff has been observed to occur at higher fields in some instances,⁴ but this could be due to surface effects^{11,12} and/or trapped space charge¹³ caused by inadequate resting of the sample.

(iii) At the high end of the electric field region, the QE is close to unity for short-wavelength excitation, whereas it is very small for long-wavelength excitation. A study of the absorption coefficient shows that the absorption is essentially complete at all these wavelengths, even in the case of the thinner film.

Before discussing what we feel are the reasons for the nature of the electric field dependence of quantum efficiency, it is appropriate to point out the explanations offered by previous investigators and the reasons for their arriving at these conclusions. The optical absorption, in common with other amorphous materials, is not sharp and is characterized by a long tail extending over at least 0.5 eV.² The exponential absorption edge described by Urbach's rule is quite common in many crystalline materials and the origin of this is still not clear. The striking feature, however, is that even when the absorption coefficient is high and the light is completely absorbed in the sample, the quantum efficiency of generation is low in the long-wavelength region. The absorption coefficient begins to drop off at about 560 nm whereas the quantum efficiency starts to fall off at 450 nm. This has led² to the concept of a gap between the absorption edge and photogeneration edge, and it has culminated in the idea of dual absorption. The quantum efficiencies were obtained by erroneously assuming that QE saturated to different values for different wavelengths at intermediate fields with no further increase at higher fields. An inspection of Fig. 2 reveals that if the measurements are terminated at 5×10^6 V/m, an illusion of saturation can be observed. The conclusion of saturation is central to the argument that there are two types of absorption, one the so-called photoconductive I_p with unity QE, and the other the so-called nonphotoconductive I_N with zero QE. The "saturation" QE at any wavelength is defined by the ratio $I_p/(I_N + I_p)$.

Any dropoff from saturation was explained in terms of bulk trapping. This idea of dual absorption has spawned many other theories,¹⁴ none of which we believe is needed to provide an explanation of the observed results.

The electric field and wavelength dependence of the QE can be satisfactorily explained as arising from the photogeneration process itself. The solid lines in Fig. 2 give the Onsager dissociation efficiency as a function of applied electric field. It should be clear even without a complete knowledge of the Onsager expression, the details of which are described in the Sec. IV, that the dissociation efficiency would be dependent on the initial distance between the two carriers. The larger the initial distance, the greater the dissociation efficiency would be for any given field. The theoretical curves of Fig. 2 are obtained for different initial distances between the carriers. The variation of QE in the middle- and high-field regions of the applied electric field arises from an Onsager-type separation of a generated pair of carriers, as evidenced by the excellent fit of the measured points with the theoretical predictions. However, the measured efficiencies fall below the theoretical Onsager predictions at the low end of the applied field region, and the reasons for this deviation will now be discussed.

We will catalog the possible mechanisms that could be operative in this low-field region and eliminate the ones not applicable. Loss due to bulk trapping has been eliminated as a possibility based on measurements made on films of different thicknesses. It has been suggested that this deviation may be due to the failure of the isotropic media theory to describe the random walk process in a locally anisotropic material such as selenium.¹⁵ Other possibilities suggested have been recombination in the generation region¹⁶ and surface recombination and/or trapping.¹¹

Recent two-photon photogeneration measurements led to the conclusion that the low-field drop is due to surface effects.¹¹ Figure 3 shows the electric field dependence of the observed efficiency for a two-photon photogeneration process using weakly absorbed radiation of 1.17-eV photon energy. This experiment has the characteristic that the absorption takes place uniformly in the bulk, but the carrier pairs are produced with twice the incident photon energy, or 2.34 eV. Figure 3 also shows the photoinjection efficiency for a strongly absorbed radiation source of 2.3-eV photon energy. The single-photon photogeneration process with the entire photogeneration taking place close to the surface shows a dropoff in efficiency at low fields, whereas the two-photon photogeneration process with its bulk absorption shows the low-field saturation extending over the entire low-field

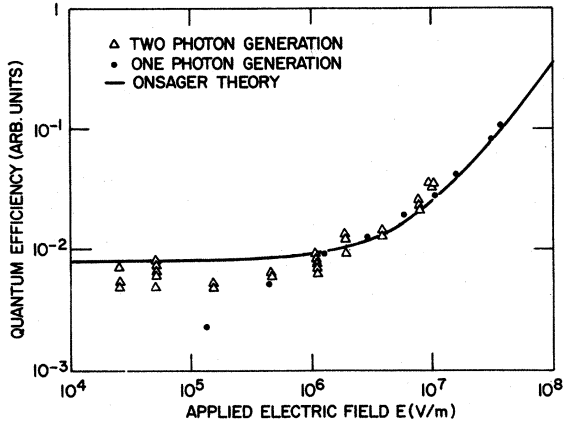


FIG. 3. Quantum efficiency of photogeneration of two photon ($2 \times 1.17 = 2.34$ eV) and single photon of 2.34-eV absorption vs electric field.

region. This result indicates that the low-field drop below saturation for single-photon excitation is due to a loss mechanism either at the surface or in the photoabsorption region.

If the loss is due to free carrier recombination in the absorption region, the linear dependence of the photoinjection efficiency over many orders of magnitude variation of light intensity shows the recombination process to be monomolecular in nature.⁴ Therefore, the recombination lifetime is independent of the carrier concentration. Since the loss is proportional to the time of transit through the absorption region, the loss would vary linearly with the absorption depth. Therefore, this predicts that the deviation from the Onsager theory would occur at higher fields for greater absorption depths. This is in conflict with the experimental

data shown in Figs. 2 and 3. The absence of bulk trapping effects associated with the recombination centers has also been used as evidence against the importance of recombination in the absorption region.⁴ These considerations show that the low-field deviation from the Onsager theory is due to either trapping or recombination of free carriers at the surface.

IV. FRENKEL VERSUS ONSAGER FORMULATIONS

The analysis of photogeneration mechanisms has generally been carried out either in the framework of Frenkel formulation⁶ or the Onsager formulation.⁷ Both these theories were proposed to explain the departure from Ohmic behavior in either weak electrolytes or solid dielectrics. The source of the field dependence in both cases arises from a reduction of the ionization energy for the separation of two charges under their mutual Coulomb attraction. The reduction in the thermal ionization energy required to separate the charge carriers results in an increase in the efficiency of dissociation with the applied electric field. The resulting expressions using the two treatments appear substantially different. In the interest of a clear understanding of the differences between the two formulations, we will attempt to sketch the outlines of the analyses.

A. Frenkel formulation

Frenkel carried out a one-dimensional analysis of electric field assisted thermal ionization of an electron under the Coulombic influences of a fixed positive charge embedded in a uniform dielectric medium. The solid line of Fig. 4 represents the potential energy of an electron about the positive nucleus in the absence of the applied electric field,

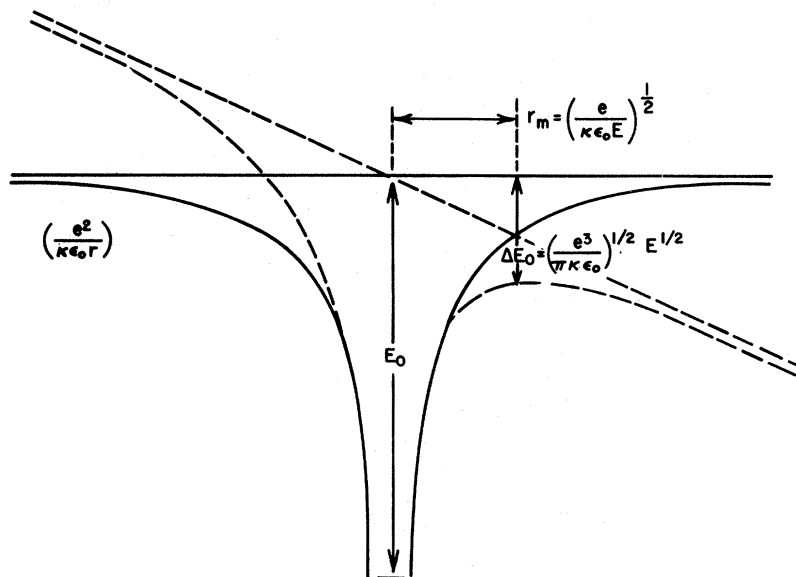


FIG. 4. Schematic of a Coulombic barrier between oppositely charged carriers being lowered by the applied electric field.

and the dashed line corresponds to the potential in the presence of the applied field.

The maximum of the potential energy U in the presence of an electric field is obtained by equating $\partial U/\partial x = 0$, and is given by

$$e^2/4\pi\kappa\epsilon_0x_0^2 = eE.$$

If E_0 is the barrier height in the absence of the applied field, the barrier in the presence of the field is given by

$$E_b = E_0 - \Delta E_0 = E_0 - \left(\frac{e^2}{4\pi\kappa\epsilon_0x_0} + eEx_0 \right) = E_0 - \beta E^{1/2}, \quad (5)$$

where

$$\beta = (e^3/\pi\kappa\epsilon_0)^{1/2}.$$

The probability of electron escape due to thermal excitation in the presence of the field is increased to

$$e^{-E_0/kT} e^{\beta E^{1/2}/kT} = e^{-E_0/kT} \left[1 + \frac{\beta E^{1/2}}{kT} + \frac{1}{2!} \left(\frac{\beta E^{1/2}}{kT} \right)^2 + \dots \right]. \quad (6)$$

Attempts have been made recently to make it complete and applicable to more meaningful situations. The expression for the probability of escape in the three-dimensional case has been derived as¹⁷

$$e^{-E_0/kT} \left\{ \left(\frac{kT}{\beta\sqrt{E}} \right)^2 \left[1 + \left(\frac{\beta\sqrt{E}}{kT} - 1 \right) e^{\beta\sqrt{E}/kT} \right] + \frac{1}{2} \right\}. \quad (7)$$

To obtain a complete expression for efficiency of dissociation which reaches unity at high fields, it is necessary to add a competing mechanism of geminate recombination. The steady-state rate equation is given by⁴

$$\frac{dN}{dt} = I_{ph} - \frac{N}{\tau_r} - \frac{N}{\tau_i} = 0, \quad (8)$$

where N is the density of excited pairs, I_{ph} is the photon flux, τ_r^{-1} is the rate of decay of an excitation through geminate recombination, and τ_i^{-1} is the rate at which excited pairs dissociate into free electron-hole pairs. Since the total rate of dissociation is N/τ_i , the efficiency of dissociation η is

$$\eta = \frac{N}{\tau_i} / I_{ph} = 1/(1 + \tau_i/\tau_r), \quad (9)$$

where $1/\tau_i = \nu e^{-E_0/kT} e^{\beta E^{1/2}/kT}$ from Eq. (6), and ν is an attempt to escape frequency.

The efficiency of dissociation is then equal to

$$\eta = [1 + (1/\nu\tau_r) e^{E_0/kT} e^{-\beta E^{1/2}/kT}]^{-1}. \quad (10)$$

B. Onsager formulation

The theory of geminate recombination (or initial recombination) reduces to the problem of Brownian motion in the presence of the Coulomb attraction

and the applied electric field. The Onsager approach is to solve the equation of Brownian motion given by

$$\frac{\partial f}{\partial t} = \frac{kT}{e} (\mu_1 + \mu_2) \text{div}(e^{-U/kT} \text{grad} f e^{U/kT}), \quad (11)$$

where μ_1 and μ_2 are the mobilities of the two charge carriers, and U is the Coulomb potential modified by the applied electric field.

In the case of stationary flow with a source at the origin and a sink at $r = \infty$, the probability of ionization is increased by

$$\frac{K(E)}{K(0)} = \frac{J_1(i\beta\sqrt{E}/kT)}{\frac{1}{2}i(\beta\sqrt{E}/kT)} = 1 + \frac{1}{2!} \left(\frac{1}{4} \frac{\beta^2 E}{k^2 T^2} \right) + \left(\frac{1}{4} \frac{\beta^2}{k^2 T^2} E \right)^2 / 2!3! + \left(\frac{1}{4} \frac{\beta^2}{k^2 T^2} E \right)^3 / 3!4! + \dots, \quad (12)$$

where J_1 is a Bessel function of the first order. This is entirely different from the expression derived by Frenkel [Eq. (6)] for the increase in the probability of ionization as a function of the applied electric field. Onsager calculated the problem of initial recombination by considering a similar problem with different boundary conditions in which the source is at infinity and the sink at $r = 0$. Using the solutions to the two extreme boundary condition problems, Onsager's relation for the probability $p(r, \theta, E)$ that an ion pair thermalized with an initial separation r and at an angle θ with the applied electric field direction will escape initial recombination is given by

$$p(r, \theta, E) = e^{-A} e^{-B} \sum_{n=0}^{\infty} \sum_{m=0}^{\infty} \frac{A^m}{m!} \frac{B^{m+n}}{(m+n)!}, \quad (13)$$

where

$$A = e^2/4\pi\kappa\epsilon_0 kT r. \quad \text{and} \quad B = (eEr/2kT)(1 + \cos\theta).$$

Here we have used the rationalized mks system and the notation used is similar to that used by Geacintov and Pope.¹⁸

If we now define ϕ_0 as the efficiency of production of thermalized ion pairs per absorbed photon and $g(r, \theta)$ as the initial spatial distribution of separation between ions of each ion pair, the overall generation efficiency will be given by

$$\phi(E) = \phi_0 \int p(r, \theta, E) g(r, \theta) d^3r, \quad (14)$$

where ϕ_0 is assumed to be independent of the applied electric field. It is reasonable to begin with the assumption that the initial distribution of thermalized pairs is an isotropic δ function, so that¹⁸⁻²⁰

$$g(r, \theta) = (1/4\pi r_0^2) \delta(r - r_0), \quad (15)$$

where r_0 is a characteristic thermalization length. Carrying out the integration in Eq. (14), the resulting expression for escape (generation) efficiency is given by

$$\phi(r_0, E) = \phi_0 \frac{kT}{eEr_0} e^{-A} \sum_{m=0}^{\infty} \frac{A^m}{m!} \sum_{n=0}^{\infty} \times \left[1 - e^{-eEr_0/kT} \sum_{l=0}^{m+n} \left(\frac{eEr_0}{kT} \right)^l \frac{1}{l!} \right]. \quad (16)$$

This can be rewritten as

$$\phi(r_0, E) = \phi_0 \frac{kT}{eEr_0} e^{-A} e^{-eEr_0/kT} \times \sum_{m=0}^{\infty} \frac{A^m}{m!} \sum_{n=0}^{\infty} \sum_{l=n+1}^{\infty} \left(\frac{eEr_0}{kT} \right)^l \frac{1}{l!}, \quad (17)$$

where $A = e^2/4\pi\kappa\epsilon_0 kTr_0$. If we now define²¹ a critical Onsager distance $r_c(T)$ as that distance at which the Coulomb energy is equal to kT ,

$$r_c(T) = e^2/4\pi\kappa\epsilon_0 kT. \quad (18)$$

The first few terms of Eq. (17) can then be written as

$$\phi(r_0, E) = \phi_0 e^{-r_c(T)/r_0} \left[1 + \left(\frac{e}{kT} \right) \frac{1}{2!} r_c E + \left(\frac{e}{kT} \right)^2 \frac{1}{3!} r_c \left(\frac{1}{2} r_c - r_0 \right) E^2 + \left(\frac{e}{kT} \right)^3 \frac{1}{4!} r_c \left(r_0^2 - r_0 r_c + \frac{1}{6} r_c^2 \right) E^3 + \dots \right]. \quad (19)$$

The expression for generation efficiency in the form of Eq. (16) has been evaluated numerically to varying degrees of approximation for comparison to experimental results in a number of organic materials. The most common approach is to keep terms only to the first order in the electric field [see Eq. (19)].¹⁹ In principle, the slope-to-intercept ratio provided by this low-field approximation can provide a sensitive test of the applicability of the Onsager theory. However, as will be discussed more fully later, serious experimental problems obstruct this test. Other approximations used involved allowing n to increase until a term tests smaller than some fraction of the sum to that point, but arbitrarily limiting m to a small number (~ 6)¹⁸ or allowing n and m to increase by steps together until the contribution from some step tests less than some fraction of the sum to that point.²⁰ This cumbersome approach is probably due to the inconvenient form in which Eq. (16) is written, which requires small differences of large numbers to be calculated.

However, when Eq. (16) is rewritten as Eq. (17), the sums are all obviously convergent and can be taken in a straightforward manner with all the upper limits determined by testing each term until one is found which is less than some fraction of the sum to that point. This has been done for amorphous selenium using a relative dielectric constant of 6.3 and a test fraction for terminating the sums of 10^{-4} . The computation was terminated

at a quantum efficiency of 0.95 due to the slow convergence between 0.95 and 1.0. The results at room temperature for the best choices of ϕ_0 and r_0 to fit experiments are shown in Fig. 2. The maximum values of the indices used in this calculation are $l=140$, $n=115$, and $m=24$. Using a test fraction of 10^{-3} gives efficiency values with a maximum fractional difference of 0.003 from those obtained using a test fraction of 10^{-4} , indicating the accuracy of the procedure.

V. DISCUSSION

Until now the variation of QE with electric field in amorphous selenium has been explained in the framework of the Frenkel formalism.³⁻⁵ Though approximate agreement between experiment and the theory has been noted, the only conclusion that has resulted is that the field dependence of generation arises from a reduction of the thermal ionization energy necessary to separate two oppositely charged carriers in their mutual Coulomb field, due to the lowering of the Coulomb barrier by the external field. The application of the Frenkel expression to the experimental data, however, has raised several questions. The Frenkel expression of Eq. (6) is at best a one-dimensional approximation to the problem of charge separation in the presence of Coulomb attraction and an applied electric field. The refinements introduced in Eq. (10) were simply meant to put an upper bound of unity to the expression derived by Frenkel. This was done at the expense of introducing several parameters such as the attempt-to-escape frequency ν , and a geminate recombination lifetime τ_r . The major disagreement between theory and experiment is in the most basic parameter β , which defines the variation of efficiency with field. The experimentally measured β are found to be approximately half the value of $(e^3/\pi\kappa\epsilon_0)^{1/2}$ predicted by the Frenkel expression. Though Frenkel's theory predicts an exponential temperature dependence of $e^{-E_0/kT}$, the magnitude of the activation energy E_0 is an additional arbitrary parameter which is not predictable from the room-temperature data.

As can be seen from the derivation of Onsager's expression for dissociation efficiency, the initial or geminate recombination is taken into account in the derivation. The only parameters that enter into the expression are r_0 , the initial distance between the oppositely charged carriers, and ϕ_0 , the fraction of absorbed photons that result in thermalized pairs of oppositely charged carriers. The initial distance r_0 determines the shapes as well as the relative magnitudes of the QE variations with field for different exciting wavelengths, whereas ϕ_0 merely translates the entire family of curves along the vertical axis. The magnitude of the temperature variation of the Onsager dissociation efficiency

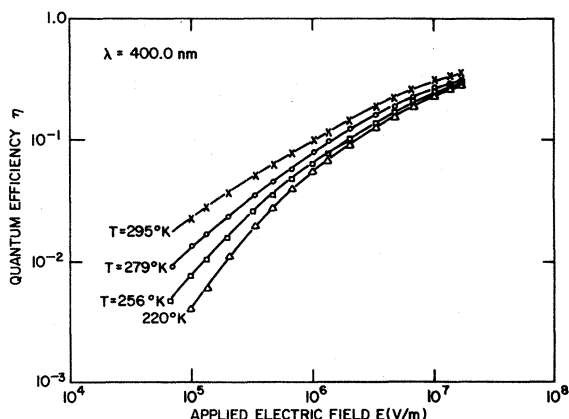


FIG. 5. Quantum efficiency of injection of holes vs electric field at several temperatures and at an exciting wavelength of 400.0 nm.

is determined by r_0 and ϕ_0 obtained by the fit to the room-temperature data assuming r_0 and ϕ_0 to be independent of temperature. This is in contrast to the arbitrariness of the magnitude of temperature dependence of the PF expression.

It is found that the room-temperature data in Fig. 2 can be best fitted with the Onsager expression for $\phi_0=1$ and for r_0 values in the range 0.84 to 7.0 nm when the excitation wavelength is changed from 620 to 400 nm. From the data on photoinjection efficiency in amorphous Se as shown in Fig. 2, it is seen that in the wide range of applied electric fields used in the experiment the shape and magnitude of the QE variation is unique at each wavelength. Hence, the fitting of the data with the Onsager expression was done without any ambiguities as to the value of r_0 and ϕ_0 required to obtain the best fit at each wavelength. The confidence in the accuracy of these values of r_0 obtained from the room-temperature data is further substantiated by the good agreement to be shown later between the measured activation energies and the ones calculated using these values of r_0 . Amorphous selenium is the only material we know of where the application of Onsager's expression yields unity value of ϕ_0 . The physical meaning of this result is that, irrespective of the exciting wavelength, each absorbed photon creates a thermalized pair of carriers, and, at a given field, a certain fraction $\eta(E)$ of them dissociate into free carriers and the remaining $[1 - \eta(E)]$ recombine. This means that even for long-wavelength excitation, the number of thermalized pairs is equal to the number of absorbed photons, while the low efficiency of production of free carriers at any field is due to the small initial distances between carriers in the thermalized pairs. This is significant in that the explanation based on dual absorption² to explain the low QE at long wavelength is inconsistent with this

result. In contrast to the unity value obtained for amorphous Se, the ϕ_0 values for anthracene¹⁹ are in the range of 10^{-3} – 10^{-4} , and that obtained for a charge transfer complex of poly(N-vinylcarbazole) and 2,4,7-trinitro-9-fluorenone²⁰ is approximately 0.25.

A. Temperature variation of quantum efficiency

The photoinjection efficiency in amorphous selenium films has also been measured as a function of electric field and temperature for exciting light of several wavelengths. The measurements are performed using the transient photoconductivity technique on electroded films. Figures 5 and 6 show the field dependence of photoinjection efficiency at different temperatures for exciting wavelengths of 400 and 580 nm, respectively. It is evident that QE is a function of both electric field and temperature. When these data were explained³ in the framework of the Poole-Frenkel formalism, an inspection of Eq. (10) revealed that an explicit activation energy could be obtained by extrapolating to $E=0$ the straight lines obtained by plotting the data on a $\log \eta$ vs \sqrt{E} plot. The Onsager relation, however, is not a straight line on a $\log \eta$ vs \sqrt{E} plot, as shown in Fig. 7, although a straight-line region can be observed over a considerable portion of the electric field range. In light of this, the activation energies calculated by extrapolating $\log \eta$ vs \sqrt{E} plot have no significance in the Onsager theory. It was observed by fitting the Onsager expression to measured data at each temperature that ϕ_0 is approximately unity, and the variation of r_0 with temperature in the region in which the measurements have been performed is small. The r_0 values obtained by fitting the measured data with the Onsager expression are shown in Table I.

Assuming that r_0 is independent of temperature

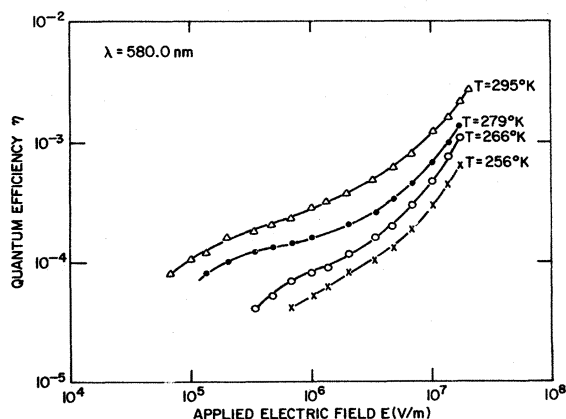


FIG. 6. Quantum efficiency of photoinjection of holes vs electric field at several temperatures and at an exciting wavelength of 580.0 nm.

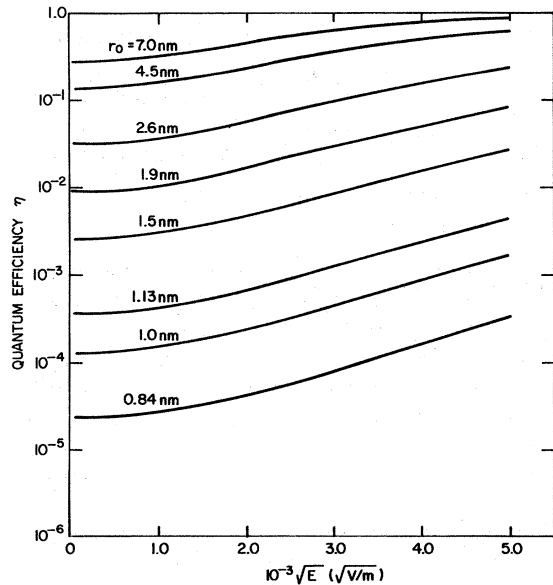


FIG. 7. Onsager dissociation efficiency vs square root of the applied electric field for several initial separations.

as indicated by the data shown in Table I, the temperature dependence of the Onsager dissociation efficiency can be computed for any photon energy. The theoretical expression predicts that the temperature dependence will be a function of the applied electric field, and this is observed experimentally. Figure 8 shows the Onsager dissociation efficiency plotted as a function of inverse temperature for several initial distances r_0 and for an applied electric field of 7×10^6 V/m. The initial distances r_0 used in this computation are the room-temperature values from Fig. 2 and are assumed to be independent of temperature. For the temperature range over which the QE has been measured, an activation energy can be defined. In Fig. 9, the computed activation energies of QE are compared with those measured at 7×10^6 V/m. For

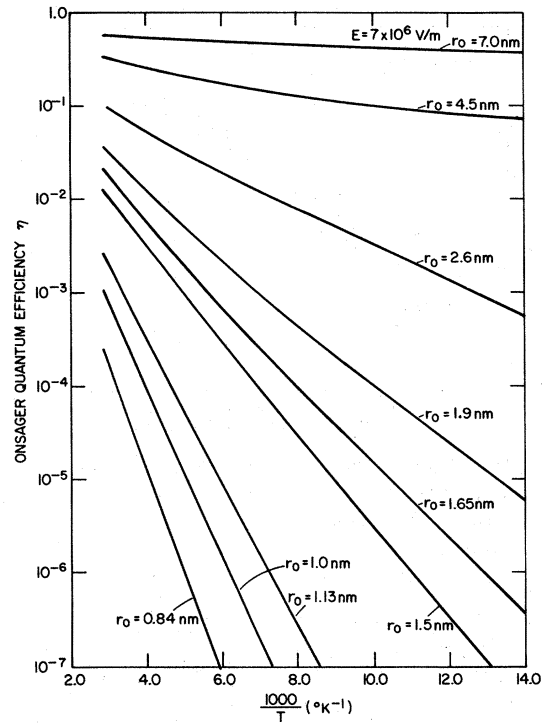


FIG. 8. Temperature dependence of the Onsager dissociation efficiency for various initial separations and at an applied electric field of 7×10^6 V/m.

short-wavelength excitation, excellent agreement is observed between the measured values and those predicted by the Onsager expression. The theoretical prediction of a rise in activation energies towards the long wavelengths is also observed, though the absolute agreement between the measured and theoretical values in this region is not as satisfactory.

Several factors can influence the activation energies in the long-wavelength region when the initial distances are small. For small initial distances, a small fractional change in r_0 as a function

TABLE I. Temperature dependence of the initial separation r_0 of charge carriers for several excitation wavelengths.^a

Excitation wavelength, λ (nm)	Initial separation r_0 (nm)				
	$T=294^\circ\text{K}$	$T=280^\circ\text{K}$	$T=268^\circ\text{K}$	$T=257^\circ\text{K}$	$T=223^\circ\text{K}$
400	7.0	7.0	...	7.0	7.0
450	5.3	5.4	...	5.2	5.2
480	4.0	...	4.19	3.97	3.6
500	3.21	3.33	3.28	3.07	3.0
520	2.52	2.4	2.56	2.45	2.39
540	2.02	2.04	2.05	1.92	1.97
560	1.44	1.38	...	1.38	1.36
580	1.23	1.22	1.23	1.19	...

^aResults obtained using electroded samples.

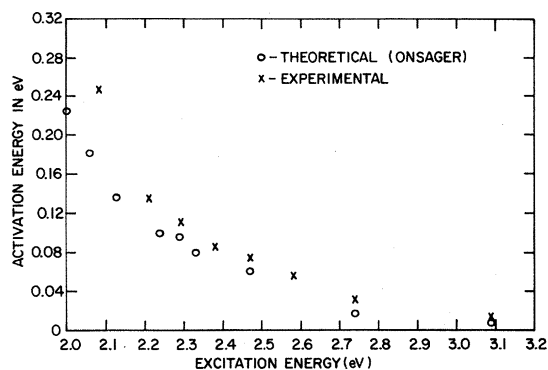


FIG. 9. Comparison of the theoretical (Onsager) and experimental values of the activation energy as a function of photon energy at an applied electric field of 7×10^5 V/m.

of temperature has a far greater influence on QE and hence the activation energy. The same fractional change in r_0 has a smaller effect for larger initial distances. Small initial separations are also the circumstances when the assumption of diffusive motion of the carrier may have to be somewhat modified. Carrier mean free paths in amorphous materials are generally assumed to be on the order of the interatomic distance. Since the smallest r_0 being considered is only a few times the interatomic separation, some effects might be expected.

B. Variation of thermalization distance with exciting wavelength and temperature

The variation of the thermalization distance r_0 with energy of the exciting radiation is plotted in Fig. 10. The assumption that the variation in r_0 with the energy of the exciting radiation occurs as a result of the variation of the initial kinetic energy of the carriers upon excitation is a reasonable one and has been applied for explaining photogeneration in liquid hydrocarbons and anthracene.^{21,22} In the absence of a more successful analysis, we will apply the treatment of Davis⁵ and Knights and Davis²³ to determine the thermalization lengths from the excess kinetic energy. Thermalization is achieved by dissipating the excess kinetic energy over the local potential by phonon emission. The motion during this process is assumed to be diffusive with a diffusion coefficient D so the thermalization distance $r_0 = \sqrt{Dt_0}$, where t_0 is defined as the thermalization time. They further assume that the rate of loss of energy by phonon emission is independent of excess energy and is given by $h\nu_p^2$, where ν_p is a typical phonon frequency. Assuming a "band gap" of E_g , the photon has an excess energy of $h\nu - E_g$ over the band edge and an excess of $h\nu - E_g + e^2/4\pi\kappa\epsilon_0r$ over the local Coulomb potential.

Knights and Davis²³ used their relation for r_0 to calculate the Poole-Frenkel binding or activation

energy of $E_0 = e^2/4\pi\kappa\epsilon_0r_0$ to compare with the experimentally measured activation energies. However, it is clear from the Onsager expression given by Eq. (19) that $e^2/4\pi\kappa\epsilon_0r_0$ represents only the zero-field activation energy. As is evident from Fig. 7, the zero-field QE in the Onsager formalism cannot be obtained by extrapolating the high-field quantum efficiency to zero field as has been done in the above analysis. In fact, the activation energy is not a suitable fundamental quantity, since it could be strongly affected by the variation of other parameters such as r_0 as well as the intrinsic temperature variation predicted by the theory. The initial separation, on the other hand, is more directly connected with the physics of the photogeneration process. With ν_p^2/D and E_g as parameters, the Knights and Davis relation has been used to fit the experimentally obtained data of r_0 vs $h\nu$ shown in Fig. 10. The dashed curve of Fig. 10 results when $\nu_p = 1.34 \times 10^{13}$ \sqrt{D} /sec and $E_g = 2.36$ eV. The second curve of Fig. 10 results when ν_p and E_g have the values 9.3×10^{12} \sqrt{D} /sec and 2.60 eV, respectively. Though the values of ν_p and E_g are not unreasonable, the fit to the experimental data in Fig. 10 is far from satisfactory. A better understanding of the motion of hot carriers in amorphous materials will have to be achieved before any great significance can be attached to the quantities derived from the experimentally observed relationship between the photon excitation energy and the thermalization distance. Even though there is no adequate theoretical explanation of the magnitude of r_0 and its variation with the excitation wavelength and temperature, the good agreement between the Onsager theory and the experimental data indicates that the values derived are physically meaningful. Even for long-wavelength excitation (small r_0), where the assumption of diffusive motion and continuous medium are most questionable, the good agreement with experiment indicates that the theory is applicable.

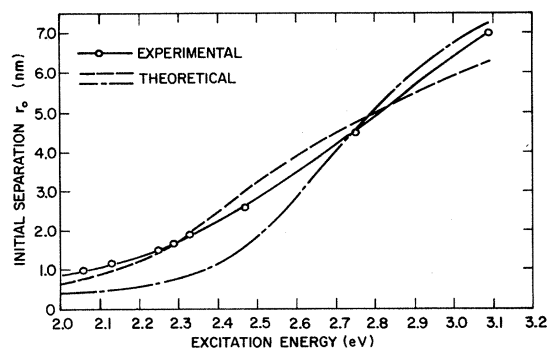


FIG. 10. Experimental initial separation distances as a function of the photon energy. Figure also shows the expected variation of initial distances using a simple model.

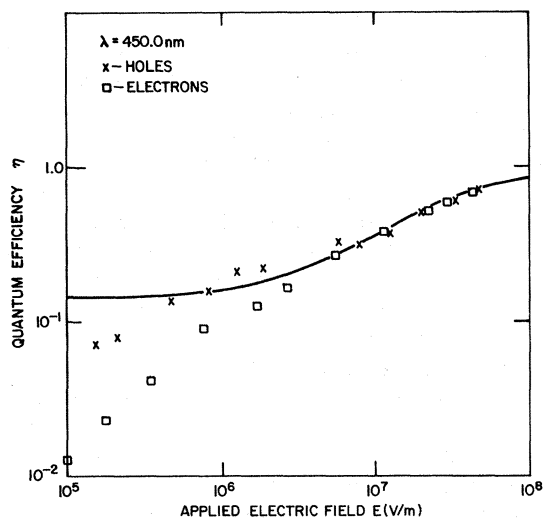


FIG. 11. Comparison of photoelectron injection efficiencies of holes and electrons as a function of the applied electric field at an exciting wavelength of 450.0 nm. The solid line is the Onsager dissociation efficiency for $\phi_0 = 1$ and $r_0 = 4.5$ nm.

Though precise experimental data are not available, there has been some discussion about the expected form of the temperature dependence of r_0 when the Onsager theory of dissociation is applied to explain the QE data in anthracene and the carrier yield data in liquid hydrocarbons. The argument²² is based on the temperature dependence of the diffusion constant. In a crystalline material such as anthracene, the temperature dependence of the mean free path resulting from the fluctuations in the lattice density causes D to have an inverse temperature dependence. The thermalization distance, which is proportional to \sqrt{D} , is expected to have $T^{-0.5}$ dependence. However, because of the disorder associated with the amorphous nature of the material, the mean free path in amorphous selenium is small, probably of the order of the interatomic distance, and the effect of phonon scattering, therefore, is expected to be small. Thus, the weak temperature dependence of r_0 displayed in Table I is not surprising.

In the literature, the validity of applying Onsager theory of dissociation to photogeneration process in anthracene^{21,24} and crystalline As_2S_3 (Ref. 25) is often checked by consideration of the slope-to-intercept ratio. This is done by taking the low-field approximation of Eq. (19) given by

$$\phi(r_0, E) \approx \phi_0 e^{-r_0(T)/r_0} \left\{ 1 + \left[\frac{e}{kT} \right] \frac{1}{2} r_0 E \right\}. \quad (20)$$

The carrier yield versus electric field plot in this region is linear and should have a slope-to-intercept value of $(e/kT) \frac{1}{2} r_0$. Good agreement with the experimentally measured slope-to-intercept ratio

has recently been found in the case of anthracene.²⁴ Using a dielectric constant of 6.3 for amorphous Se, it is seen from Eq. (19) that the E^2 term has a value of 10% of the E term at a field of 1.7×10^6 V/m; hence the approximation of Eq. (20) is valid for QE data points for fields below 10^6 V/m.

However, as can be seen from Fig. 2, the fit between the measured injection efficiency for amorphous Se and the Onsager expression deteriorates below 10^6 V/m, and the slope-to-intercept test will not be attempted here. In view of the excellent fit of the measured efficiencies with the Onsager expression for fields larger than 10^6 V/m, there should be no doubt as to the validity of the application of the Onsager theory of dissociation to photogeneration in amorphous Se. Recent experimental results¹² have shed much light on why the measured photoelectron injection efficiencies are lower than those predicted by the Onsager expression in the field region below 10^6 V/m. It is found that the photogeneration is indeed that predicted by the Onsager theory, but that the measured injection efficiencies are less by the amount of loss due to diffusion back to the surface of the photogenerated carriers followed by either trapping or recombination at the surface.

VI. ELECTRON QUANTUM EFFICIENCY RESULTS

The Onsager theory of dissociation predicts equal quantum efficiency of generation for both holes and electrons, since the escape of the hole from the Coulomb field of the electron also implies the escape of the electron from the influence of the hole. However, the bulk deep trapping lifetime of electrons is more sensitive to the presence of some impurities; hence extreme care must be exercised to ensure that the electron injection efficiencies are not affected by bulk trapping. Figures 11 and 12 show the comparison between injection efficiencies of electrons and holes at room temperature and at exciting wavelengths of 450 and 540 nm, respectively. The theoretical Onsager dissociation efficiencies for the appropriate r_0 is also shown in the figures. The hole and electron quantum efficiencies of injection are the same in the region where the measured injection efficiencies are equal to those predicted by the Onsager theory of dissociation. They are different, however, in the low-field region where the generated carriers diffuse back to the surface and are subject to loss either by trapping or recombination on the surface. The nonequality between the electron and hole injection efficiency is probably due to the differences in trapping and recombination kinetics of the surface for electrons and holes. One other interesting feature of Figs. 11 and 12 is that the departure from the predicted Onsager efficiency occurs at higher field for 450-nm excitation. This observa-

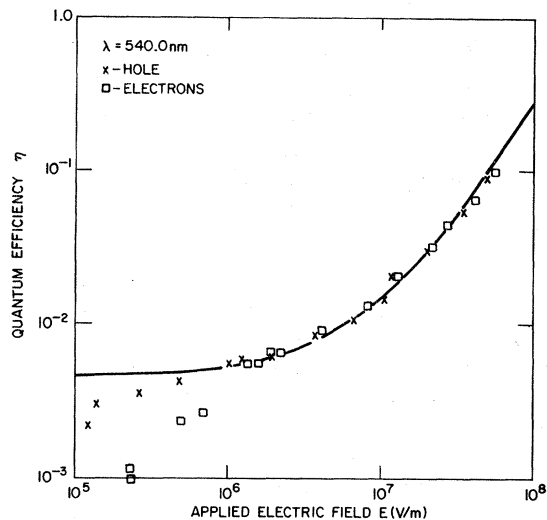


FIG. 12. Comparison of photoinjection efficiency of holes and electrons as a function of the applied electric field at an exciting wavelength of 540.0 nm. Solid line is the Onsager dissociation efficiency for $\phi_0=1$ and $r_0=2.02$ nm.

tion is consistent with the picture of surface effects causing the low-field dropoff, since the absorption coefficient is larger for 450-nm excitation; hence the free carrier generation takes place closer to the surface.

VII. CONCLUSIONS

We have shown that the Onsager theory of dissociation explains satisfactorily the electric field,

excitation wavelength, and temperature dependence of photogeneration in amorphous selenium. Though photogeneration data in several liquid hydrocarbons, anthracene, poly(N-vinylcarbazole), and 2,4,7-trinitro-9-fluorenone, have been explained on the basis of the Onsager formulation, the data on photogeneration in amorphous selenium presented in this paper is the most complete and unambiguous demonstration of the power of the Onsager theory in explaining the photogeneration data. The excellent fit between the experimental data and the theory over a very wide range of initial separations provides proof of the validity of the assumption of isotropic distribution of initial separations. We have further shown that irrespective of the exciting wavelength, each absorbed photon creates a thermalized pair of carriers and the low efficiency of production of free carriers at long wavelengths is due to the shorter initial separations. This result invalidates the explanation of the so-called "nonphotoconductive edge" in amorphous selenium on the basis of dual absorption. Though it is reasonable to assume that the variation of the initial separation distances with wavelength of the exciting radiation occurs as a result of the variation of the kinetic energy of the carriers upon excitation, the fit of the measured values of the initial distances with those provided by a simple model is not satisfactory.

ACKNOWLEDGMENT

The authors are grateful to James Neyhart of Xerox Corporation who supplied some of the xerographic discharge data used in this paper.

¹H. T. Li and P. J. Regensburger, *J. Appl. Phys.* **34**, 1730 (1963).

²J. L. Hartke and P. J. Regensburger, *Phys. Rev.* **139**, A970 (1965).

³D. M. Pai and S. W. Ing, *Phys. Rev.* **173**, 729 (1968).

⁴M. D. Tabak and P. J. Warter, Jr., *Phys. Rev.* **173**, 899 (1968).

⁵E. A. Davis, *J. Non-Cryst. Solids* **4**, 107 (1970).

⁶J. Frenkel, *Zh. Tekh. Fiz.* **5**, 685 (1938); *Phys. Rev.* **54**, 647 (1938).

⁷L. Onsager, *Phys. Rev.* **54**, 554 (1938); *J. Chem. Phys.* **2**, 599 (1934).

⁸W. E. Spear, *Proc. Phys. Soc. Lond. B* **70**, 669 (1957).

⁹J. L. Hartke, *Phys. Rev.* **125**, 1177 (1962).

¹⁰R. M. Blakney and H. P. Grunwald, *Phys. Rev.* **159**, 664 (1967).

¹¹R. C. Enck, *Phys. Rev. Lett.* **31**, 220 (1973).

¹²R. C. Enck, *Bull. Am. Phys. Soc.* **211**, 19 (1974).

¹³M. E. Scharfe and M. D. Tabak, *J. Appl. Phys.* **40**, 3230 (1969).

¹⁴G. Lucovsky and M. D. Tabak, *Selenium*, edited by

R. A. Zingaro and W. C. Cooper (Van Nostrand Reinhold, New York, 1974), p. 788.

¹⁵P. J. Warter, *Proceedings of the Third International Conference on Photoconductivity* (Pergamon, New York, 1971), p. 311.

¹⁶H. Seki, *Phys. Rev. B* **2**, 4877 (1970).

¹⁷J. L. Hartke, *J. Appl. Phys.* **39**, 4871 (1968).

¹⁸N. E. Geacintov and M. Pope, in Ref. 15, p. 289.

¹⁹R. H. Batt, C. L. Braun, and J. F. Horning, *J. Chem. Phys.* **49**, 1967 (1968); *Appl. Opt. Suppl.* **3**, 20 (1969).

²⁰P. J. Melz, *J. Chem. Phys.* **57**, 1694 (1972).

²¹A. Mozumdar and J. L. Magee, *J. Chem. Phys.* **47**, 939 (1967).

²²M. Silver and R. C. Jarnagin, *Mol. Cryst. Liq. Cryst.* **3**, 461 (1968).

²³J. E. Knights and E. A. Davis, *J. Phys. Chem. Solids* **35**, 543 (1974).

²⁴R. C. Chance and C. L. Braun, *J. Chem. Phys.* **59**, 2269 (1973).

²⁵D. F. Blossey and R. Zallen, *Phys. Rev.* **9**, 4306 (1974).